The Kellerjoch Gneiss (Tyrol, Eastern Alps): An Ordovician pluton with A-type affinity in the crystalline basement nappes north of the Tauern Window

Peter TROPPER[1] [*], Friedrich FINGER[2], Erwin KRENN[2], Urs KLÖTZLI[3], Andreas PIBER[1] & Sonja GANGL[1]

[1] Institute of Mineralogy and Petrography, University of Innsbruck, Innrain 52, A-6020 Innsbruck, Austria;

[2] Department of Geography, Geology and Mineralogy, University of Salzburg, Helbrunnerstrasse 54, A-5020 Salzburg, Austria;

[3] Department of Lithospheric Research, University of Vienna, Althanstrasse 14, A-1090 Wien, Austria;

[*] Corresponding author: peter.tropper@uibk.ac.at

Abstract

The Kellerjoch Gneiss (KG, Schwazer Augengneis) is part of the Austroalpine basement nappes north of the Tauern Window and extends from Schwaz in the West to Wörgl in the East. It is tectonically intercalated between the Innsbruck Quartzphyllite Nappe in the footwall and the Greywacke Zone in the hanging wall. Microscopical observations imply that the KG is a shallow intruded porphyroitic metagranite. Embayed phenocrysts of quartz and simple twins of K-feldspar phenocrysts with diameters up to more than 1.5 cm support this interpretation. Remnants of the magmatic paragenesis are K-feldspar + albitic plagioclase + Ti-rich biotite. The latter show recrystallization (Variscan or eo-Alpine?) to Ti-poor biotite and a Ti phase (rutile, ilmenite, titanite). The eo-Alpine metamorphic paragenesis consists of muscovite + biotite + albite + chlorite ± stilpnomelane and mineral compositions indicate eo-Alpine metamorphic conditions around 300-400 °C and 5-7 kbar. TIMS single zircon U-Pb dating yielded concordia ages of 468 ± 1 Ma and 469 ± 1 Ma (± 2 SD) for two samples of the KG, respectively, interpreted as the igneous formation age. Zircons extracted from a meta-pegmatite with the mineral assemblage garnet$_1$ (alm-rich) + garnet$_2$ (grs-rich) + chlorite + stilpnomelane + albite + quartz, crosscutting the Kellerjoch Gneiss, are slightly younger with a U-Pb concordia age of 462 ± 1 Ma. A strongly mylonitizised orthogneiss (Stengelgneis) which occurs adjacent to the KG gave a slightly higher zircon U-Pb concordia age of 475 ± 1 Ma. The most common accessory minerals in the KG are monazite, allanite, apatite, zircon and xenotime. Based on textural investigations, two generations of monazite can be distinguished. Primary monazite form crystals with diameters of 40 μm. Some of these monazites are replaced by a corona of apatite and allanite, which indicates a (Variscan?) metamorphic overprint. Secondary monazite occurs as small-scale grains with a diameter of 5-10 μm mostly within the cleavage of muscovite and biotite and intergrown with rutile or ilmenite. Occasionally, secondary monazite is intergrown with xenotime, in which case formation temperatures of <400°C can be inferred from monazite-xenotime miscibility gap thermometry. Electron microprobe-based U-Th-Pb dating of primary monazite yielded CHIME (chemical Th-U-total Pb isochron method) ages of 465 ± 22 Ma and 469 ± 34 Ma, which are in good agreement with the zircon ages. Due to low Th, U, Pb-contents it was not possible to date the small secondary monazite grains. However, based on textural evidence their growth during the eo-Alpine event is likely. Additionally, the low yttrium contents correlate well with low-grade P-T conditions. With regard to the age of its protolith, the KG is another important example of the prominent Lower Ordovician magmatic event, which is found in many places throughout the Austroalpine. While most of these Lower Ordovician magmas are I-type or S-type, the KG is special in that it shows geochemically an A-type affinity.

Der Kellerjochgneis (KG, Schwazer Augengneis) ist Teil der austroalpinen Basementdecken nördlich des Tauern Fensters und erstreckt sich von Schwaz im Westen bis nach Wörgl im Osten. Tektonisch liegt er zwischen dem Innsbrucker Quarzphyllit im Liegenden und der Grauwackenzone im Hangenden. Es handelt sich um einen seicht intrudierten porphyrischen Metagranit. Die magmatischen Relikte sind K-Feldspar + albitreicher Plagioklas + Ti-reicher Biotit. Letzterer rekristallisierte (variszisch oder eoalpidisch?) zu Ti-armen Biotit und einer Ti-Phase (Rutil, Ilmenit, Titanit). Die eoalpine Mineralparagenese besteht aus Muskovit + Biotit + Chlorit ± Stilpnomelan und die eoalpinen P-T Bedingungen waren ca. 300-400 °C und 5-7 kbar. TIMS U-Pb Datierung von Einzelzirkonen ergab Concordia-Alter von 468 ± 1 Ma und 469 ± 1 Ma (± 2 SD) welche als Intrusionsalter interpretiert werden. Zirkone aus einem diskordantem Metapegmatit mit der Mineralparagenese Granat1 (alm-reich) + Granat2 (grs-reich) + Chlorit + Stilpnomelan + Albite + Quarz ergaben ein jüngeres U-Pb Alter von 462 ± 1 Ma. Der starker mylonitisierte Stengelgneis ergab ein U-Pb Alter von 475 ± 1 Ma. Die häufigsten akzessorischen Mineralphasen im KG sind Monazit, Allanit, Apatit, Zirkon und Xenotim. Basierend auf texturellen Beobachtungen konnten zwei Generationen von Monazit unterschieden werden: Primärer Monazit bildet ca. 40 μm grosse Körner und wird oft von Apatit und Allanit im Zuge einer späteren (variszischen?) Metamorphose umgewandelt. Sekundäre Monazite treten als kleine Körner mit einem Durchmesser von 5-10 μm in den Spaltflächen von Muskovit und Biotit oft auch mit Rutil oder Ilmenit verwachsen auf. Manchmal sind sie auch mit Xenotim verwachsen was auf Bildungstemperaturen von ca. <400°C mittels Monazit-Xenotim Solvusgeothermometrie hinweist. U-Th-Pb Elektronenstrahlmikrosondendatierung von primären Monaziten er-

gab sog. CHIME (chemical Th-U-total Pb isochron method) Alter von 465 ± 22 Ma und 469 ± 34 Ma, welche mit den U-Pb Altern aus den Zirkonen sehr gut übereinstimmen. Wegen der geringen Th, U, Pb-Gehalte war es aber nicht möglich die sekundären Monazite zu datieren. Ihr texturelles Auftreten in der eoalpinen Hauptschieferung weist aber auf ein eoalpines Wachstum hin. Die niedrigen Y-Gehalte weisen ebenfalls auf ein niedriggradiges P-T Ereignis hin. Basierend auf den geochronologischen Daten stellt der KG ebenfalls ein weiteres Mitglied der Unter-Ordovizischen Magmatite dar, die im Austroalpin weit verbreitet sind. Im Gegensatz zu den meisten Unter-Ordovizischen I-Typ oder S-Typ Graniten weist der KG geochemisch eine ausgeprägte A-Typ Affinität auf.

1. Introduction and geographical overview

Metagranitoid rocks are widespread in the Austroalpine nappes north of the Tauern Window (e.g. Schönlaub, 1980; Rockenschaub et al., 1999, 2003). They occur as low-grade metamorphosed porphyric gneisses mostly in the vicinity of quartzphyllites. One of the largest bodies is the Kellerjoch-gneiss (KG) (Schwazer Augengneiss), which extends from Schwaz in the West to the Wildschönau (S of Wörgl) in the East. Ordovician magmatism is generally typical for the Greywacke Zone (e.g. Gangl et al., 2005; Heinisch, 1981; Löschke, 1989; Neubauer et al., 2002; Schauder, 2002; Söllner et al., 1997) and correlations between the KG in the western Greywacke Zone and the Blasseneck porphyry in the Eastern Greywacke Zone were based on geochemical and geochronological data (Heinisch, 1981; Heinisch and Schmidt, 1982; Roth, 1983; Söllner et al., 1997; Gangl et al., 2005; Berberich and Heinisch, 2008, Blatt, 2013). We contribute to this discussion by presenting geochemical data and zircon and monazite ages from the KG crystalline basement nappe north of the Tauern Window.

2. Geological Overview

The polymetamorphic crystalline basement north of the Tauern Window consists of lower Ordovician porphyroid-gneisses (Kellerjochgneiss KG/Schwazer Augengneiss), micaschists (Patscherkofel Crystalline Complex) and Paleozoic schists (Innsbruck Quartzphyllite Complex, IQP, and Wildschönau Schists) with intercalated carbonate rocks (Schwaz Dolomi-te) as shown in Figure 1. These lithologies are in a hanging wall position relative to the lithological units of the Tauern Window. Since the late 19th century (Pichler, 1868) the KG was the subject of geological investigations. In the second half of the 20th century the tectonic position of the KG was contro-versially debated. Tollmann (1963, 1977, 1986) defined the KG as an Alpine nappe and attributed it together with the Stein-kogelschiefer and Patscherkofel-Crystalline Complex (PCC) to the so-called Middle Austroalpine unit, whereas other authors interpreted it to be the base of the inverted Innsbruck Quart-zphyllite and thus to be of Lower Austroalpine origin (Schmi-degg, 1954, 1964; Gwinner, 1971). According to the new tec-tonic subdivision of Schmid et al. (2004) the KG together with the IQP is considered to be part of the Upper Austroalpine Silvretta-Seckau nappe system.

The first quantitative P-T data of the KG were obtained by Satir and Morteani (1978 a,b) and Satir et al. (1980), who con-cluded, based on the Si-content of white micas, that pressures reached 5.3 kbar in the KG. Temperatures were estimated with stable isotope thermometry, based on ^{18}O-^{16}O fractionation between phengite and quartz, and yielded a temperature of 403°C. Satir and Morteani (1978b) interpreted these P-T con-ditions to represent the Variscan metamorphic event. Based on this interpretation, the authors concluded that the condi-tions of the eo-Alpine metamorphic overprint did not exceed 350°C and 2-3 kbar. More recently Piber and Tropper (2003 a,b, 2005, 2007, 2010) and Piber et al. (2009) published selected geothermobarometric data of the KG which yielded eo-Alpi-ne P-T conditions ranging from 4 to 8 kbar and 300-400°C. The results of the most recent stu-dy of Tropper and Piber (2012) show that the P-T data ob-tained with different thermo-dynamic databases and me-thods yield consistent results and converge at ca. 5-7 kbar and 300-400°C.

Satir and Morteani (1978a) conducted the first geochro-nological investigations of the KG. They obtained a protolith intrusion age of the orthog-neisses of 425 Ma based on a whole-rock Rb-Sr isotope stu-dy. Blatt (2013) investigated KG samples with respect to zircon
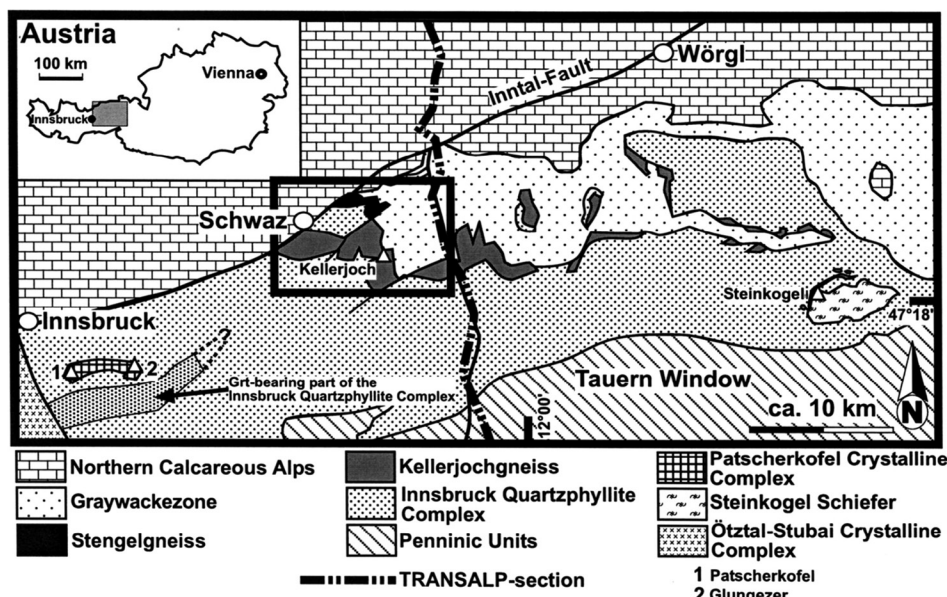
Figure 1: Geological overview of the basement nappes north of the Tauern Window. Note the TRANSALP section in the center of the image.
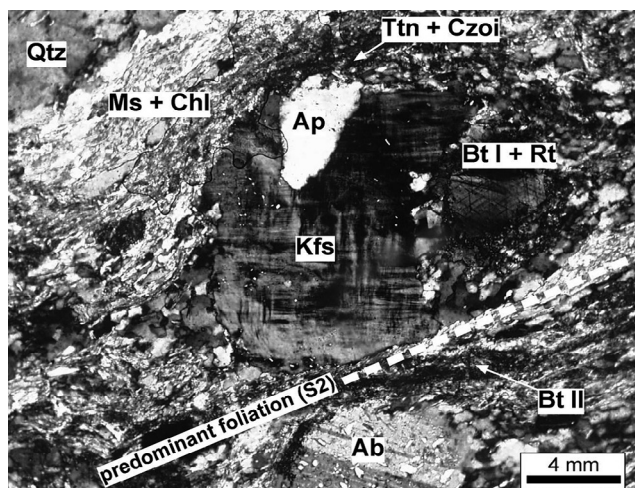
Figure 2: Photomicrograph of the characteristic mineral assemblage of the augen-bearing Kellerjochgneiss with relic K-feldspar (Kfs) and albite porphyroblasts, magmatic biotite (Bt) with rutile (Rt) inclusions occurring as sagenite grid and chlorite (Chl) and muscovite (Ms). On the top of the picture at the rim of the K-feldspar, titanites (Ttn) and clinozoisites (Czoi) occur (X Nichols, magnification 4x) (sample A-19).

geochronology. He obtained a wide scatter of the resulting U-Pb ages with inherited zircon cores showing Pan-African (Cadomian) ages, but also Proterozoic and Palaeozoic ages. He determined concordia-ages of augengneiss and porphyroid samples, which plot in a time span from 471 to 469 Ma and 465 to 464 Ma and interpreted them as the age of the magmatic intrusions. Only samples from the aplitic intrusions gave younger ages between 462 and 461 Ma, confirming a pegmatite age described by Piber et al. (2009). Based on the Pan-African (Cadomian) ages of the inherited zircon cores, Blatt (2013) assumes a paleogeographical position of the Northern Greywa-

cke Zone at the northern Gondwana margin. Satir and Morteani (1978a) also reported a Variscan Rb-Sr whole-rock age of 322 ± 24 Ma for the KG. Rb-Sr data on phengites from the KG yielded Permian cooling ages of 260 and 273 Ma. Based on Th-U-Pb electron microprobe data for monazite and thorite, Steyrer and Finger (1996) obtained ages of 453 ± 26 Ma (considered as magmatic formation age) and 323 ± 9 Ma (Variscan metamorphism). In addition, there are a few data constraining the low-temperature evolution of the KG. Definite eo-Alpine ages are still missing from the KG, only strongly disturbed Ar-Ar age patterns with Cretaceous ages in the low-temperature increments were observed (Handler et al., 2000).

3. Lithological and petrographical description

The rocks of the KG occur as mylonitic augengneisses containing large feldspar porphyroclasts with diameters of up to 3.5 cm. The colour of these rocks is gray. A strong cataclastic overprint locally occurs. Although metaporphyric gneisses occur showing frequently embayed quartz and granophyric intergrowths of K-feldspar and quartz, which are indications for a shallow depth of magmatic crystallization (Piber, 2002, 2005), only orthogneisses (samples A19, S20A) without these features were used in this study. The main mineral assemblage of the KG is muscovite + biotite + chlorite + albite-rich feldspar + quartz (Fig. 2). Former Ti-rich magmatic biotite now contains abundant inclusions of Ti-bearing phases (titanite, rutile) (Piber, 2002, 2005). In addition, clinozoisite and stilpnomelane occur. Subordinately secondary calcite appears locally. Accessory minerals are titanite, ilmenite, rutile, allanite, apatite, monazite, zircon and xenotime. Strongly mylonitized parts of the KG containing the same mineral assemblage are called Stengelgneiss (sample A 106).
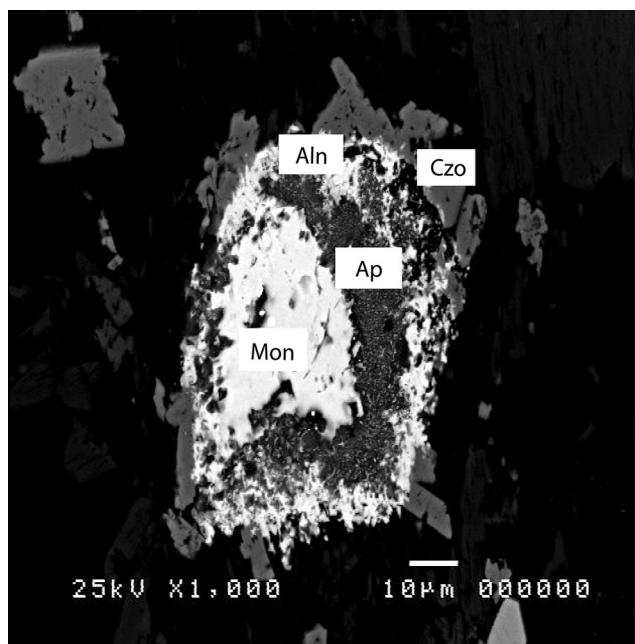
Figure 3: Backscatter electron (BSE) image of first generation monazite (Mon) replaced by allanite (Aln)/epidote (Czo) and apatite (Ap). The matrix consists of albite and muscovite Sample A19.
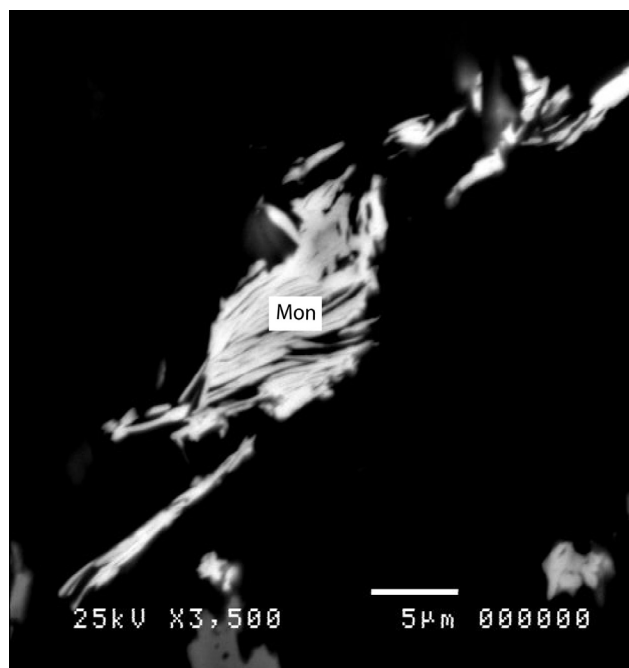
Figure 4: Backscatter electron (BSE) image of second generation monazite (Mon) lamellae within biotite. Sample A19.

Based on textural investigations, two generations of monazite can be distinguished. A first generation of monazite occurs as xenomorphic crystals with diameters of 40 μm. Occasionally, these monazites are replaced by a corona of apatite and allanite (Fig. 3). The second generation of monazites occurs as small-scale grains with a diameter of 5-10 μm within the cleavage of muscovite and biotite (Fig. 4) as well as intergrown with rutile or ilmenite and together with apatite. Occasionally, secondary monazites coexist with xenotime. Detailed compositional data of the mineral assemblage except for monazite can be found in Tropper and Piber (2012).

Within the Kellerjochgneiss a small, crosscutting, strongly deformed meta-pegmatite dike occurs (sample A77; Piber et al., 2009). Field relations indicate that the pegmatite intersects the Kellerjochgneiss discordantly. The pegmatite contains the mineral assemblage muscovite + biotite + albite + chlorite + quartz + garnet1 ($Alm_{68}Spess_{27}Pyr_3Gro_2$) + garnet$_2$ ($Gros_{52}Alm_{33}Spess_{15}$) ± stilpnomelane (Piber et al., 2009). Textural investigations reveal a protolith assemblage comprised of K-feldspar, quartz and garnet. The composition of garnet1 is comparable to garnet compositions from other pegmatites from the Eastern Alps (e.g. Koralpe Crystalline complex; Thöni et al., 2008; Campo Complex; Sölva et al., 2003).

4. Analytical methods

4.1 EMPA

Back-scatter electron (BSE) images were obtained with a JEOL X-8100 electron microprobe at the Institute of Mineralogy and Petrography of the University of Innsbruck. Operation conditions were 15 kV at a sample current of 10 nA. U, Th and Pb analyses for EMPA U-Th-Pb dating were performed on a JEOL JX 8600 at the Department of Geography and Geology at the University of Salzburg. In order to obtain precise Th, U and Pb concentrations, long counting times were used (Th Ma: 20s, U Ma: 30s and Pb Ma: 140 s), at a high beam current of 200 nA and 15 kV accelerating voltage. Under these conditions the typical 2s errors for Th, U and Pb are 0.05 wt.%, 0.04 wt.% and 0.007 wt. % respectively. The beam diameter was slightly defocused to about 2 μm to avoid beam irradiation effects (Jercinovic and Williams, 2005). Slight interferences of Th on U, and Y and Th on Pb, were empirically corrected with standards. Further details of the analytical procedure are also outlined in Finger and Helmy (1998).

4.2 U/Pb isotope analysis

Zircon pre-chemistry handling (air-abrasion, cleaning) for all U/Pb analyses followed procedures given in Klötzli et al. (2001). U/Pb chemistry and mass spectrometric analysis followed a slightly modified vapor digestion procedure originally described by Wendt and Todt (1991) and Klötzli et al. (2001). The Pb isotopic composition and U and Pb concentrations were determined using a Finnigan MAT 262 multi-collector thermal ionization mass spectrometer. Pb fractionation, derived from NIST SRM 981 and 982 standard measurements, was

0.11 % per mass unit (± 23 %). U fractionation was corrected using U500 standard measurements (0.082 % per mass unit; ± 15 %). U/Pb analyses were controlled by replicate analyses of standard zircon 91500 (Wiedenbeck et al., 1995). External reproducibility for U/Pb analysis based on the 91500 standard measurements is 0.2 % for $^{207}Pb/^{206}Pb$ (0.07494 ± 0.00015) and 0.25 % for $^{206}Pb/^{238}U$ (0.17972 ± 0.00045).

The total procedural Pb blank was 2 ± 1 pg. The corresponding U blank was below 0.1 pg. Age calculation and error statistics were made using "Rockage" (Parrish et al., 1987) and the "Isoplot/Ex" software (Ludwig, 2003). All errors reported are 2 standard deviations. Common Pb corrections were made using model Pb isotopic ratios from Stacey and Cramers (1975) recalculated to the apparent $^{207}Pb/^{206}Pb$ age.

4.3 Whole-rock geochemistry

Sixteen large samples from different exposures of the Kellerjochgneiss were analyzed by means of XRF and ICP-MS methods. XRF analyses were carried out on glass beads and powder pellets at the University of Innsbruck. ICP-MS analyses were carried out at the Centre de Recherches Petrographiques et Geochimiques in Vandoeuvre. Rock powders were first fused to $LiBO_2$ glass, which was then dissolved in HNO_3.

5. Results

5.1 Mineral chemistry of monazite

Table 1 shows representative electron microprobe analyses of 4 primary and 6 secondary monazites. The chemical difference between both groups lies mostly in CaO, Y_2O_3, Nd_2O_3, ThO_2 and PbO. While primary monazites show higher values with respect to CaO, Y_2O_3, ThO_2 and PbO, secondary monazites show higher Nd_2O_3 contents. The very low PbO contents of 0.01 wt.% inhibited a meaningful age calculation for secondary monazites.

5.2 Whole-rock geochemistry

Analytical results are reported in Tables 2A and 2B, together with typical analytical uncertainties and detection limits.

	A19	A19	A19	A19	S13	S13	S13	S13	S13	S13
SiO_2	0.23	0.22	0.23	0.23	0.14	0.32	0.26	1.42	1.85	1.95
Al_2O_3	n.d.	n.d.	n.d.	n.d.	0.02	0.15	0.02	0.88	0.94	1.02
P_2O_5	29.85	29.40	29.89	29.55	29.94	29.26	27.70	29.45	29.12	29.35
CaO	1.08	1.03	1.07	1.10	0.11	0.10	0.10	0.46	0.53	0.57
Y_2O_3	2.57	2.70	2.51	2.61	1.19	0.81	0.34	0.55	0.47	0.44
La_2O_3	13.23	13.01	13.44	13.33	15.90	16.18	15.19	15.35	15.16	15.02
Ce_2O_3	31.29	30.92	30.85	30.84	35.57	35.72	34.71	35.42	35.06	35.37
Pr_2O_3	4.40	4.29	4.34	4.38	5.20	5.27	4.99	4.88	4.82	4.77
Nd_2O_3	10.69	10.58	10.53	10.58	11.39	11.57	11.77	11.00	11.06	11.06
ThO_2	5.46	5.46	5.32	5.28	0.59	0.34	0.93	1.70	1.64	1.62
UO_2	0.16	0.15	0.15	0.13	0.14	0.09	0.04	0.07	0.06	0.09
PbO	0.13	0.11	0.10	0.11	n.d.	0.01	n.d.	0.01	n.d.	n.d.
Total	99.07	97.87	98.43	98.13	100.19	99.82	96.05	101.21	100.71	101.26
Si	0.009	0.009	0.009	0.009	0.005	0.012	0.010	0.053	0.069	0.072
P	0.991	0.989	0.994	0.990	0.990	0.977	0.972	0.950	0.940	0.939
Al	n.d.	n.d.	n.d.	n.d.	0.001	0.007	0.001	0.039	0.041	0.044
Ca	0.044	0.043	0.044	0.046	0.004	0.004	0.004	0.018	0.021	0.023
Y	0.052	0.056	0.051	0.054	0.024	0.017	0.007	0.011	0.009	0.009
La	0.187	0.186	0.190	0.190	0.224	0.230	0.227	0.211	0.208	0.205
Ce	0.449	0.450	0.444	0.447	0.509	0.516	0.527	0.494	0.489	0.490
Pr	0.061	0.061	0.061	0.062	0.072	0.074	0.073	0.066	0.065	0.064
Nd	0.146	0.146	0.144	0.146	0.155	0.159	0.170	0.146	0.147	0.146
Th	0.048	0.048	0.046	0.046	0.005	0.003	0.009	0.014	0.014	0.014
U	0.001	0.001	0.001	0.001	0.001	0.001	0.000	0.001	0.000	0.001
Pb	0.001	0.001	0.001	0.001	n.d.	<0.001	n.d.	n.d.	<0.001	n.d.

Monazite formulae calculated on the basis of 2 O; A19: primary monazites; S13: secondary monazites

Table 1: Electron microprobe analyses of primary and secondary monazites

|	A85	A56	A87	S54	S57	A91	S56	S79	A98	S33B	A19	S20A	S5	S84	S44	t.a.u.	d.l.
SiO_2	66.78	67.05	67.31	67.79	68.38	68.49	69.32	69.82	69.97	70.12	70.25	70.39	70.82	71.08	71.3	< 1	0.1
Al_2O_3	15.33	15.5	14.73	15.12	14.26	14.89	14.57	15.27	14.56	14.19	14.31	14.38	15.65	14.1	14.21	< 3	0.1
Fe_2O_3	5.39	4.01	4.91	2.98	3.84	3.66	3.73	3.25	3.6	3.18	3.97	3.52	2.98	3.81	3.49	< 3	0.1
MnO	0.05	0.04	0.05	0.03	0.06	0.04	0.04	0.03	0.06	0.04	0.05	0.03	0.01	0.02	0.06	< 10	0.01
MgO	1.68	1.23	1.34	0.8	0.8	1.17	0.79	0.94	0.84	0.67	1.04	0.69	0.72	0.69	0.62	< 5	0.05
CaO	0.31	1.38	1.28	1.84	1.49	1.26	0.62	0.33	0.96	1.45	0.51	0.49	0.18	0.77	0.49	< 5	0.1
Na_2O	3.35	2.61	3.32	3.88	3.17	3.62	2.98	3.38	4.09	3.06	3.29	2.94	2.09	3.66	2.96	< 3	0.1
K_2O	4.16	4.08	3.58	4.4	4.82	3.65	5.34	4.74	3.33	4.82	4.57	5.34	4.78	3.81	5.24	< 3	0.1
TiO_2	0.69	0.63	0.69	0.45	0.46	0.53	0.42	0.39	0.47	0.41	0.5	0.4	0.4	0.36	0.35	< 10	0.01
P_2O_5	0.29	0.32	0.3	0.24	0.24	0.26	0.23	0.24	0.23	0.21	0.26	0.21	0.17	0.22	0.22	< 10	0.01
L.O.I.	1.73	2.88	2.45	2.27	2.26	2.42	1.67	1.52	1.91	2.01	1.35	1.18	2.05	1.63	1.15		
Total	99.76	99.73	99.96	99.8	99.78	99.99	99.71	99.91	100.02	100.16	100.1	99.57	99.85	100.15	100.09		
A/CNK	1.45	1.38	1.26	1.04	1.09	1.22	1.23	1.35	1.21	1.10	1.27	1.25	1.75	1.22	1.24		

Major elements in wt. %, LOI= l oss on ign ition; n.d .= not dete cted; d.l. = detectio n limit; t.a .u.= typic al analytic al uncerta inty (in % rel.)

Table 2 A: X-ray Flourescence major element analyses of the Kellerjoch Gneiss, ordered according to increasing SiO_2 content

	A85	A56	A87	S54	S57	A91	S56	S79	A98	S33B	A19	S20A	S5	S84	S44	t.a.u.	d.l.
As	2.8	23.0	3.1	1.0	n.d.	6.8	2.0	n.d.	6.8	2.2	8.2	1.7	4.3	2.4	n.d.	< 20	0.70
Ba	613.0	832.0	532.0	660.0	608.0	485.0	518.0	498.0	406.0	529.0	503.0	566.0	387.0	332.0	454.0	< 5	3.00
Be	3.7	2.7	3.7	3.8	2.6	3.1	3.0	3.5	3.0	3.9	4.3	3.2	3.4	3.0	3.5	< 10	1.50
Bi	n.d.	0.4	n.d.	n.d.	n.d.	0.1	n.d.	n.d.	0.4	0.1	0.1	n.d.	0.1	0.1	0.1	< 25	0.80
Cd	n.d.	n.d.	n.d.	n.d.	n.d.	n.d.	n.d.	n.d.	n.d.	n.d.	n.d.	n.d.	n.d.	n.d.	n.d.		0.30
Ce	65.3	104.0	101.0	113.0	114.0	98.7	119.0	111.0	86.1	92.3	84.5	106.0	128.0	93.5	96.8	< 5	0.05
Co	9.4	8.3	8.4	3.0	5.0	5.7	3.9	1.6	5.7	4.0	6.8	4.4	4.0	5.5	4.4	< 15	0.30
Cr	32.0	27.2	33.6	13.0	15.3	20.7	11.9	11.4	18.8	12.8	18.3	12.8	6.4	9.9	10.3	< 15	5.00
Cs	4.9	6.8	4.9	4.2	5.2	2.6	6.4	2.6	3.0	2.1	5.4	3.7	7.7	4.6	4.1	< 15	0.20
Cu	12.5	12.6	9.4	n.d.	n.d.	14.8	n.d.	n.d.	25.9	n.d.	15.4	n.d.	n.d.	7.9	5.1	< 25	5.00
Dy	5.0	5.3	6.3	6.7	7.5	6.6	6.5	6.8	5.8	6.7	4.9	7.1	7.5	4.6	6.1	< 7	0.05
Er	3.0	2.6	3.3	3.8	3.8	3.6	3.5	3.7	3.2	3.7	2.9	3.7	4.0	2.6	3.5	< 7	0.04
Eu	0.8	1.2	1.2	1.2	1.3	1.1	1.2	1.0	1.1	0.8	0.7	1.1	1.3	0.8	0.9	< 10	0.02
Ga	22.6	23.0	21.8	21.4	20.4	21.2	20.1	21.6	20.0	20.9	21.3	19.7	23.3	19.4	20.4	< 5	0.13
Gd	5.2	7.1	7.3	7.6	8.5	6.8	7.6	6.6	6.0	6.2	4.4	7.2	7.6	5.3	6.7	< 6	0.10
Ge	1.5	1.1	1.6	1.7	1.7	1.5	1.8	1.7	1.3	1.8	1.7	1.9	2.5	1.8	1.9	< 15	0.10
Hf	6.8	6.7	6.9	7.1	6.3	6.5	6.9	6.3	6.0	5.9	6.7	6.1	7.1	6.0	6.0	< 5	0.04
Ho	1.1	1.0	1.2	1.4	1.4	1.4	1.3	1.4	1.3	1.3	1.0	1.3	1.4	1.0	1.2	< 5	0.01
In	n.d.	n.d.	n.d.	n.d.	n.d.	n.d.	n.d.	n.d.	n.d.	n.d.	n.d.	n.d.	n.d.	n.d.	n.d.		0.10
La	27.6	49.4	49.4	57.2	66.6	50.2	60.8	55.1	43.8	45.9	31.4	55.9	62.0	47.5	47.7	< 5	0.09
Lu	0.5	0.4	0.6	0.6	0.7	0.5	0.5	0.6	0.5	0.6	0.5	0.6	0.6	0.5	0.6	< 15	0.01
Mo	n.d.	n.d.	0.6	n.d.	n.d.	0.6	n.d.	0.8	1.7	n.d.	n.d.	n.d.	1.2	0.9	0.7	< 25	0.40
Nb	22.3	16.6	23.0	31.7	26.8	25.9	28.3	27.7	23.4	28.6	29.7	28.9	33.8	25.6	28.7	< 5	0.10
Nd	27.5	44.2	43.1	46.8	49.1	41.7	47.1	42.6	37.4	34.5	28.2	44.0	48.4	37.3	36.5	< 5	0.10
Ni	15.8	12.1	13.3	7.8	7.9	9.4	6.0	5.9	9.8	5.4	9.4	6.6	5.3	6.2	n.d.	< 25	5.00
Pb	31.0	7.9	19.5	32.7	20.9	22.0	38.0	16.2	53.3	24.4	23.2	12.8	33.6	37.9	27.6	< 8	0.90
Pr	6.9	11.4	11.1	13.0	13.6	11.6	13.8	12.3	10.0	9.7	7.7	12.3	13.5	10.4	10.3	< 5	0.04
Rb	161.0	133.0	142.0	122.0	152.0	117.0	173.0	140.0	124.0	152.0	185.0	173.0	208.0	175.0	194.0	< 5	0.60
Sb	0.9	2.8	1.0	0.3	0.3	0.9	0.5	0.4	1.2	0.4	0.8	0.5	1.6	0.6	0.4	< 15	0.10
Sm	5.4	8.6	8.2	9.0	9.3	8.0	9.4	8.7	7.2	7.0	5.8	8.9	8.9	6.8	7.1	< 10	0.06
Sn	3.8	4.2	3.6	1.5	3.5	4.3	4.5	2.8	7.5	2.3	4.4	3.3	6.3	5.4	3.5	< 10	0.50
Sr	30.7	46.6	55.0	147.0	76.9	65.4	51.6	49.1	62.3	86.9	39.6	59.8	31.9	41.4	62.9	< 10	4.00
Ta	1.9	1.4	2.0	2.8	2.3	2.4	2.4	2.5	2.1	2.6	2.7	2.4	3.1	2.4	2.8	< 6	0.03
Tb	0.8	1.0	1.1	1.2	1.3	1.1	1.2	1.1	1.0	1.1	0.8	1.2	1.2	0.9	1.0	< 7	0.01
Th	19.0	17.7	18.0	27.1	22.4	23.3	30.5	26.3	22.9	24.0	24.4	24.4	32.7	24.8	23.8	< 7	0.10
Tm	0.5	0.4	0.5	0.6	0.6	0.6	0.6	0.6	0.5	0.6	0.5	0.6	0.6	0.4	0.6	< 15	0.01
U	3.3	4.3	2.8	2.4	3.1	3.3	2.9	3.9	3.0	2.9	4.3	2.4	4.7	4.6	5.2	< 8	0.07
V	62.3	50.8	62.8	33.2	32.6	43.4	30.2	28.3	38.9	28.5	41.0	28.2	24.2	24.2	23.2	< 10	1.50
W	2.4	1.6	1.9	0.5	1.1	3.0	1.2	1.0	4.3	1.1	2.9	0.9	4.5	0.9	1.1	< 15	0.10
Y	32.7	29.0	37.1	40.0	47.5	36.5	36.1	39.0	35.1	40.1	28.5	38.9	44.1	30.4	37.4	< 5	0.05
Yb	3.2	2.5	3.6	4.2	4.2	3.9	3.7	3.9	3.2	4.1	3.1	4.1	4.4	2.8	3.7	< 5	0.03
Zn	81.3	52.0	63.1	30.0	34.7	41.9	58.0	32.0	75.7	36.9	69.2	43.6	61.7	40.6	53.9	<5	6.00
Zr	271.0	269.0	274.0	259.0	245.0	239.0	247.0	237.0	231.0	213.0	257.0	232.0	262.0	224.0	214.0	< 6	0.70

Trace and RE elements in ppm; n.d.= not detected; d.l. = detection limit; t.a.u.= typical analytical uncertainty (in % rel.)

Table 2 B: ICP-MS trace element analyses of the Kellerjoch Gneiss

Major elements: The analyses cover a relatively small, moderately acidic SiO_2 range from 66 to 72 wt.% (Table 2A). Concentrations of K, Na, Ca and mesonorm calculations (Mielke and Winkler, 1979) imply, in general, a monzogranitic protolith composition, although few sample with higher normative plagioclase amounts tend towards granodiorite. A/CNK values are strongly variable and range from mildly to strongly peraluminous (1.04 to 1.75).

Trace elements: Some trace elements like Rb, Sr are also known to be mobile during metamorphism and the measured values must therefore be treated with caution. However, immobile trace elements like Zr, Nb, Y may help to characterize

the KG in terms of its igneous petrogenesis (Table 2B). Two features are notable in this context. The first is the relatively high Zr content of the rock in the range of 200-280 ppm as shown
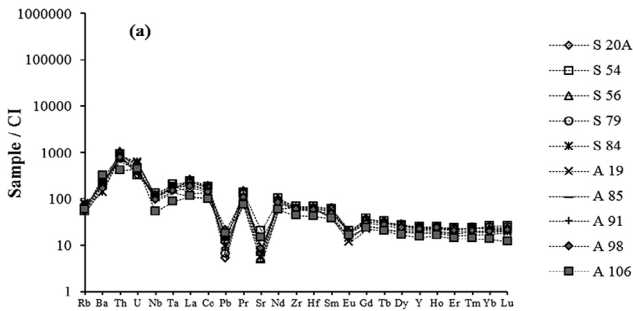
Figure 5 A: Plot of trace element variations of augengneiss samples normalized to CI (McDonough and Sun, 1995). All samples show a similar elemental distribution pattern.
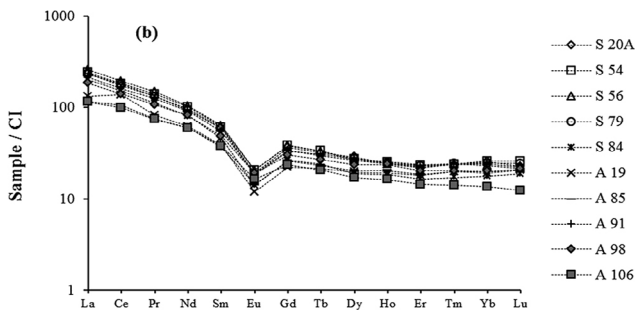
Figure 5 B: Plot of REE variations of augengneiss samples normalized to CI (McDonough and Sun, 1995). Again all samples show the distinct Eu-anomaly.
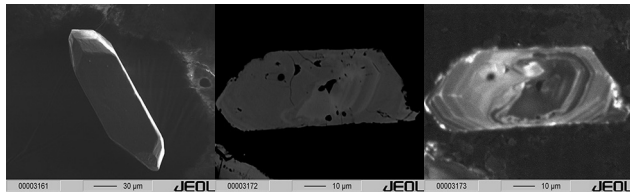
Figure 6: Secondary (SE, left), BSE (middle) and cathodoluminescence (CL, right) images of a zircon from sample A19.

in Figure 5A. The second notable geochemical feature of the KG is its high Nb content, which ranges – with two exceptions – from 20 to 36 ppm (Fig. 5A). The REE patterns of the KG are fairly uniform and consist of a fractioned LREE part, a moderately deep Eu anomaly and flat HREE tails (Fig. 5B).

5.3 Zircon and monazite geochronology

Zircons were separated from 4 samples and a typical zircon from sample A19 is shown in Figure 6. According to the classification of Pupin (1980) the zircons fall into the typology groups P2, P3, S8 and L3. The zircons only show magmatic oscillatory zoning. No later metamorphic overgrowth can be seen in CL- and BSE images. Table 3 shows the results of U-Pb TIMS dating of the 4 samples. Samples A19 and S20A represent the KG, sample A106 represents the Stengelgneiss and sample A77 is the aplitic pegmatite crosscutting the KG.

In sample A19 3 out of the 5 analyzed zircon yield a U-Pb concordia age of 468 ± 1 Ma. The remaining two crystals show minor amounts of inheritance and, respectively, lead loss (Fig. 7). Sample S20A shows major zircon inheritance and only 2 out of the 5 zircons analyzed define a U-Pb concordia age of 469 ± 1 Ma (Fig. 7). The adjacent Stengelgneiss sample A106 is a strongly mylonitizised gneiss having a U-Pb concordia age of 475 ± 1 Ma. The aplitic pegmatite (A77) yields a distinctly younger U-Pb concordia age of 462 ± 1 Ma (3 out of 4 crystals; Fig. 8).

EMPA Th-U-Pb dating of monazite: Th-U-Pb dating of primary monazite with the electron microprobe yielded weighted average ages of 465 ± 22 Ma for sample A19 and 469 ± 34 Ma for sample A87 (errors are at 95 % confidence level). Results are shown in Figure 9 and Table 4. Due to the low Pb-contents, it was not possible to date the small, secondary monazites. At least relative age information can be inferred since these monazites occur in the cleavage planes of biotites, which form the eo-Alpine foliation. To monitor the quality of the dating procedure, monazite grains with a precisely known concordant U-Pb TIMS age of 341 Ma (standard F5) have been repeatedly measured together with the specimen. A weighted

Sample Name	U (ppm)	± 2 SD (%)	Pb (ppm)	± 2 SD (%)	$^{206}Pb/^{204}Pb$	± 2 SD (%)	$^{207}Pb*/^{235}U$	± 2 SD (%)	$^{206}Pb*/^{238}U$	± 2 SD (%)	$^{207}Pb*/^{206}Pb*$	± 2 SD (%)	$^{208}Pb*/^{206}Pb*$	± 2 SD (%)	Age ± 2 SD
A106-A	13.28	0.06	1.01	1.26	1512.6	16.45	0.5965	0.96	0.07630	0.30	0.056703	0.40	0.1036	0.59	479
A106-B	68.96	0.02	5.28	1.23	1136.5	2.26	0.5974	0.22	0.07645	0.22	0.056678	0.10	0.1070	0.12	±1.5
A19-A	6.56	0.08	0.62	1.32	69.9	1.21	0.5919	1.71	0.07598	0.36	0.056495	0.70	0.3993	0.26	468
A19-B	6.74	0.07	0.61	1.21	82.8	0.94	0.5852	1.41	0.07523	0.33	0.056422	0.51	0.3429	0.23	±0.83
A19-C	11.42	0.07	0.98	1.22	91.7	0.97	0.5867	1.00	0.07525	0.35	0.056548	0.41	0.2736	0.20	
A19-D	10.62	0.07	0.85	1.22	87.5	0.81	0.5870	0.93	0.07535	0.34	0.056498	0.37	0.1710	0.28	
A19-E	14.52	0.06	1.10	1.23	367.1	1.67	0.5818	0.59	0.07471	0.25	0.056473	0.19	0.1227	0.18	
A77-A	14.06	0.06	1.24	1.23	14.06	0.06	0.5754	0.81	0.07416	0.29	0.5754	0.81	0.07416	0.29	462
A77-B	20.71	0.04	1.71	1.21	20.71	0.04	0.5772	0.91	0.07433	0.30	0.5772	0.91	0.07433	0.30	±0.83
A77-C	17.73	0.05	1.50	1.21	17.73	0.05	0.5783	0.99	0.07443	0.32	0.5783	0.99	0.07443	0.32	
A77-D	12.10	0.06	0.90	1.27	12.10	0.06	0.5806	1.07	0.07467	0.36	0.5806	1.07	0.07467	0.36	
S20A-A	25.64	0.08	4.81	2.17	60.7	2.19	1.9667	0.23	0.18382	0.27	0.077597	1.17	0.1088	1.76	469
S20A-B	13.34	0.06	1.02	1.21	363.1	18.50	0.5872	0.51	0.07521	0.71	0.056819	2.56	0.1141	2.36	±1.9
S20A-C	9.80	0.05	1.08	1.44	2194.5	157.31	0.6877	0.37	0.08104	0.85	0.061550	1.77	0.4726	0.74	
S20A-D	14.50	1.90	1.44	1.00	157.0	45.00	0.7047	0.16	0.07888	0.43	0.064790	0.01	0.3986	0.14	
S20A-E	79.20	0.02	5.84	2.40	846.1	11.99	0.5870	0.11	0.07542	0.27	0.056450	0.55	0.0990	0.64	

Table 3: Laser ICP-MS isoptopic data and ages of the zircons
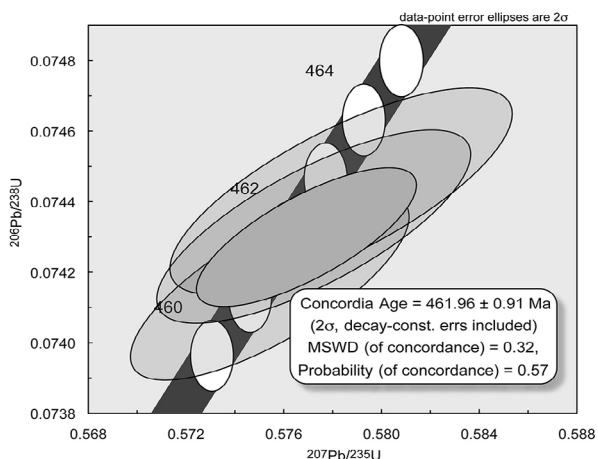
Figure 8: Plot of $^{206}Pb/^{238}U$ vs. $^{207}Pb/^{235}U$ of aplite dike sample A77.
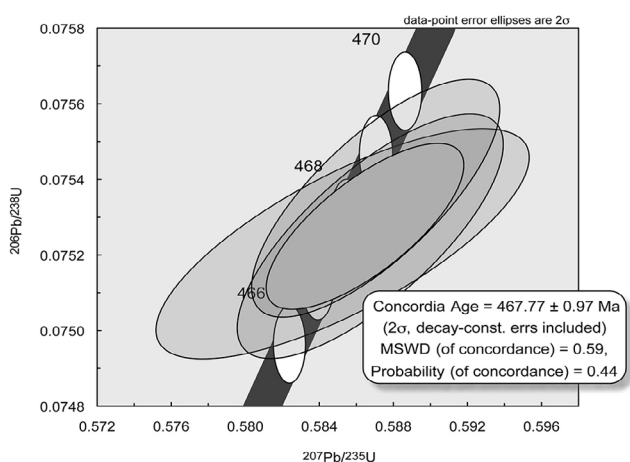
**Figure 7:** Plot of $^{206}Pb/^{238}U$ vs. $^{207}Pb/^{235}U$ of augengneiss sample A19.
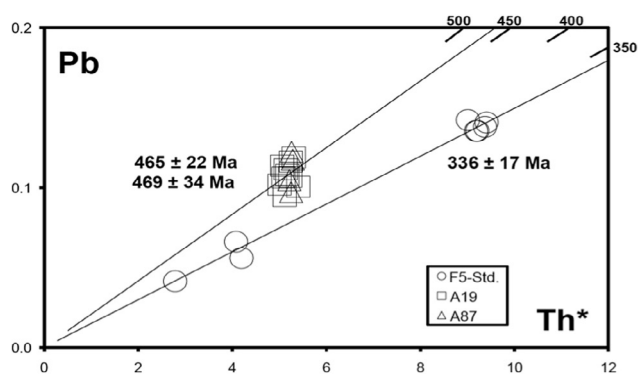
Figure 9: Pb-Th* plot of electron microprobe dating of primary monazites from samples A19 and A87. The ages of 336 ± 17 Ma represent monazite standard F5.

average age of 336 ± 17 Ma was obtained for this monazite age standard (Fig. 9).

6. Discussion

6.1 Geochemical implications

At least the highest A/CNK values are most likely an effect of element mobility during metamorphism rather than a

Sample	Th	U	Pb	Th*	Alter		Error
a19m1_1	4.619	0.144	0.106	5.091	466	±	70
a19m1_1	4.666	0.154	0.108	5.172	466	±	69
a19m1_2	4.798	0.153	0.119	5.303	500	±	67
a19m1_2	4.891	0.156	0.101	5.400	416	±	66
a19m1_3	4.638	0.130	0.114	5.066	500	±	70
a19m1_3	4.701	0.133	0.112	5.137	484	±	69
A 19 m1.1/1	4.796	0.137	0.116	5.247	494	±	68
A 19 m1.1/2	4.796	0.132	0.107	5.228	455	±	68
A 19 m1.2/1	4.674	0.133	0.095	5.110	414	±	70
A 19 m1.2/2	4.640	0.111	0.102	5.005	455	±	71
					465	*±*	*22*
a87/1-2c-m1	4.597	0.201	0.122	5.259	519	±	68
a87/1-2c-m1	4.614	0.195	0.097	5.250	414	±	68
a87/1-2c-m2	4.691	0.181	0.118	5.286	496	±	67
a87/1-2c-m2	4.614	0.183	0.105	5.213	448	±	69
					469	*±*	*34*

Table 4: U-Th*-Pb EMPA ages of monazites

primary rock feature. Taking the highest A/CNK values as an argument to characterize the KG as S-type granite may, therefore, be improper. Covariations of the major elements with the SiO₂ broadly fit with typical igneous trends (e.g. decrease of Al_2O_3, FeO, MgO, CaO, TiO_2; increase of K_2O), but there is a considerable scatter in these trends, which is most likely due to slight element mobility during metamorphism. As stated above the Zr content is clearly higher than the average S- or I-type granites (King et al., 1997, Chappell, 1999, Chappell and Hine, 2006) and Zr shows a negative correlation with the SiO_2. Such negative $Zr-SiO_2$ trends are a widely reported feature in granitic plutons and commonly explained in terms of magma differentiation through fractional crystallization (Chappell et al., 1998). High Zr contents in felsic granites can at least qualitatively be interpreted as reflecting high magma temperatures (Watson and Harrison, 1983, Chappell et al., 1998, Miller et al., 2003), and are, thus, typical for many A-type granites (Bonin, 2007).

Our geochemical study suggests an A-type granite affinity for the KG protolith. This conclusion is mainly based on elevated Zr and Nb contents, which lie above values typical for felsic I-and S-type granite as shown in Fig. 10. Berberich and Heinisch (2008) reported a mean chemical composition for the KG, which is in good agreement with our results (Fig. 10). These authors also suggested that the KG is chemically widely equivalent to porphyry rocks of the Greywacke Zone, termed "Blasseneck Porphyroide". This may hold true for the Blasseneck porphyroids of the Kitzbühel area, studied by Berberich and Heinisch (2008). However, when plotting the KG data against Blasseneck porphyroids from the Styrian type locality (Löschke 1989), the match is not too good and the latter have, for instance, clearly lower Zr and Nb contents than the KG (Fig. 10). Nb contents above 20 ppm are uncommon in both S-type and I-type granites and, in combination with the high Zr content, support an A-type granite classification for the granitic protolith of the KG.

Another argument in favor of an A-type granite classification is the high LREE contents (130-230 ppm) as shown in Figure 5B, while Y is not particularly high (24-48 ppm) and lower than in many other A-type granites. Also, the KG does not show the increased Ga/Al ratios seen in many peraluminous A-type granites (King et al., 1997). Nb, Th and Rb show a positive correlation with the SiO_2 (Tab. 2B) and appear to have behaved incompatible during magmatic differentiation. Most other trace elements (e.g. Ba, V, Zn, Sr) tend to decrease with the SiO_2. The Eu anomaly is not deepening with decreasing total REE contents, which implies that feldspar fractionation probably played no great role in magma evolution.

It is interesting to compare the composition of the KG with literature data for other Ordovician granites from central Europe. Mainly with respect to its relatively high Nb and Zr content (Fig. 10), the KG is fairly special among these rocks. The Ordovician period is commonly considered as the time when large parts of future Variscan Europe rifted off from the Gondwana margin (Von Raumer et al. 2013; see also Blatt 2013). However, S-type and I-type granite magmatism is predominant in that time span, and A-type granites are not particularly abundant, although these would be actually typical for rift settings (Bonin 2007). The occurrence of rift-related A-type granite is also in agreement with the geochemical and geochronological data of metagabbros, metabasalts and metadiorites by Schauder (2002) who obtained geochemical intraplate basalt signatures and intrusion ages of 474-469 Ma. The KG, together with the Tieftalgneiss from the Kaunertal (Bernhard et al. 1996) could thus be a rare example of an Ordovician A-type granite in central Europe.

It remains to be mentioned that Ordovician magmatism is not only reported from the Northern Greywacke Zone (Area of Kitzbühel, Zeller Furche, Radmer, Blasseneck Ratschengraben, Area of Eisenerz and Hohe Veitsch) but also from nappes south of the Tauern Window namely the Thurntaler Quartzphyllite, Marteller Quartzphyllite, Brixner Quartzphyllite and the Comelico Area (Heinisch, 1981). It could be a goal for future studies to perform a geochemical study also on these rocks.

6.2 Ordovician geochronology of the Upper Austroalpine basement north of the Tauern Window

Single zircon U/Pb analyses from this study yield U-Pb concordia ages of 468 ± 1 Ma and 469 ± 1 Ma for the KG. Zircon ages of a meta-pegmatite crosscutting the KG, are slightly younger (462 ± 1 Ma). The electron microprobe monazite ages (465 ± 22 Ma for sample A19 and 469 ± 34 Ma for sample A87) are in good agreement with these isotopic zircon ages. Our data thus corroborate the zircon age determinations of Blatt (2013) for the KG. In his data set, two separate age clusters were found for augengneisses (471 to 469) and porphyroids (465 to 464 Ma) within the KG. The first group is in excellent agreement with our data. Similar to our data are also the ages for the aplitic intrusions given in Blatt (2013). The available age dates thus suggest an overall duration of the magmatic activity of approximately 10 Ma from the early to the middle Ordovician.
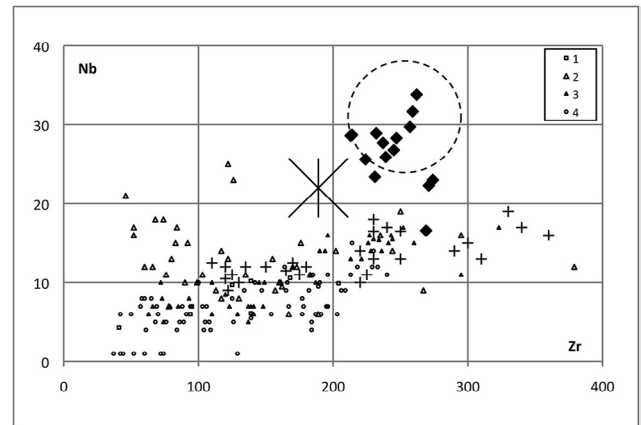
Figure 10: Zr vs. Nb diagram with plots of Kellerjoch Gneiss from this study (black diamonds). The circle approximately outlines the data cluster of Berberich and Heinisch (2008) for the Kellerjoch gneiss. The large star is the mean value for the Blasseneck porphyroids from Berberich and Heinisch (2008), the crosses are Blasseneck porphyroids from Löschke (1989). Shown for comparison are Zr-Nb data for Ordovician granitoid rocks from 1) the Gföhl gneiss in Lower Austria (unpubl. University of Salzburg data) 2) the Ötztal crystalline complex (Schindlmayr, 1999), 3) the Mont Blanc and Aiguilles Rouges basement (Von Raumer and Bussy, 2004), 4) the Fichtelgebirge, Saxothuringian Zone (Siebel et al., 1997).

6.3 Geothermometry using REE-bearing phosphates

Monazite and xenotime are important accessory phases in metamorphic and igneous rocks (e.g., Spear and Pyle, 2002). Occurring in a range of metamorphic lithologies and settings, these phosphates have great utility as prograde index minerals that can be used for geochronology and geothermometry (e.g. Harrison et al., 2002; Janots et al., 2008, 2009). They represent important reservoirs for rare-earth elements (REE), and the exchange of REE between orthophosphates and silicates such as garnet provides information about metamorphic history (Gratz and Heinrich, 1997; Andrehs and Heinrich, 1998; Pyle and Spear, 1999, 2000; Pyle et al., 2001). The monazite-xenotime geothermometer by Gratz and Heinrich (1997) is based on the T-dependent miscibility gap between monazite and xenotime and considers the LREE and HREE exchange between both. Primary monazite form crystals with diameters of 40 mm. Although no HREE besides Y were analyzed, the Y concentrations indicate limiting minimum crystallization temperature of ca. 500-550°C based on the monazite-xenotime geothermometer by Gratz and Heinrich (1997). Some of these monazites are replaced by a corona of apatite and allanite (see Fig. 3), which may have formed during fluid-influx and late-stage decompression of the Variscan metamorphic overprint (Finger et al., 1998; Broska et al., 2005; Ondrejka et al., 2012). Secondary monazite occurs as small-scale grains with a diameter of 5-10 mm mostly within the cleavage of muscovite and biotite (see Fig. 4) and intergrown with rutile or ilmenite. Occasionally, secondary monazite is intergrown with xenotime, in which case formation temperatures of <400°C can be inferred from Y concentrations based on monazite-xenotime miscibility gap geothermometry. This would be in agreement with the eo-Alpine P-T conditions of ca. 5-7 kbar and 300-400°C suggested by Tropper and Piber (2012).

7. Conclusions

The geochemical and geochronological investigations of the Kellerjochgneiss (KG, Schwazer Augengneis) yielded an A-type granite affinity for the KG protolith. This conclusion is mainly based on elevated Zr and Nb contents, which lie above values typical for felsic I-and S-type granite. U-Pb dating of zircons yielded concordia ages of 468 ± 1 Ma and 469 ± 1 Ma (± 2 SD). Therefore, with regard to its protolith and its age the KG is another important example of the prominent Early Ordovician magmatic event, which is found in many places throughout the Austroalpine. While most of these Early Ordovician magmas are I-type or S-type, the KG is special in that it shows an A-type affinity.

Acknowledgements

References

Andrehs, G. and Heinrich, W., 1998. Experimental determination of REE distributions between monazite and xenotime: potential for temperature-calibrated geochronology. Chemical Geology, 149, 83-96.

Berberich, T. and Heinisch, H., 2008. Geochemischer Vergleich von Blasseneck-Porphyroiden und Kellerjochgneisen aus den Kitzbüheler Alpen/Österreich. Geotectonic Research, Special Issue TSK 12 Abstracts, 13-16.

Bernhard, F., Klötzli, U.S., Hoinkes, G. and Thöni, M., 1996. Constraints on the age and origin of a polymetamorphic felsic intrusion in the Ötztal Crystalline Basement, Austria. Mineralogy and Petrology, 58, 171-196.

Blatt, A.K.H., 2013. Geochronologische Datierung des Kellerjochgneises und der Porphyroide in der nördlichen Grauwackenzone (Tirol, Österreich). Unpublished Ph.D. Thesis, Martin Luther University Halle-Wittenberg, 109 p.

Bonin, B., 2007. A-type granites and related rocks: evolution of a concept, problems and prospects. Lithos, 97, 1-29. http://dx.doi.org/10.1016/j.lithos.2006.12.007

Broska, I., Williams, C.T., Jank, M. and Nagy, G., 2005. Alteration and breakdown of xenotime-(Y) and monazite-(Ce) in granitic rocks of the Western Carpathians, Slovakia. Lithos 82, 71-83. http://dx.doi.org/ 10.1016/j.lithos.2004.12.007

Chappell, B.W., 1999. Aluminium saturation in I- and S-type granites and the characterization of fractionated haplogranites. Lithos, 46, 535-551.

Chappell, B.W., Bryant, C.J., Wyborn, D., White, A.J.R. and Williams, I.S., 1998. High- and Low-Temperature I-type Granites. Resource Geology, 48, 225-235.

Chappell, B.W. and Hine, R., 2006. The Cornubian Batholith: an Example of Magmatic Fractionation on a Crustal Scale. Resource Geology, 56, 203-244. http://dx.doi.org/10.1111/j.1751-3928.2006.tb00281.x

Finger, F., and Helmy, H.M., 1998. Composition and total-Pb model ages of monazite from high-grade paragneisses in the Abu Swayel area, southern Eastern Desert, Egypt. Mineralogy and Petrology, 62, 269-289.

Finger, F., Broska, I., Roberts, M.P., and Schermaier, A., 1998. Replacement of primary monazite by apatite-allanite-epidote coronas in an amphibolite facies granite gneiss from the eastern Alps. American Mineralogist, 83, 248-258.

Gangl, S., Piber, A., Tropper, P., Klötzli, U., Finger, F. and Mirwald, P. W. 2005. Geochemical evidence for Lower Ordovician magmatism in the crystalline nappes north of the Tauern Window, Geophysical Abstracts, 7, 03975.

Gratz, R. and Heinrich, W., 1997. Monazite – xenotime thermobarometry: Experimental calibration of the miscibility gap in the binary system $CePO_4 – YPO_4$. American Mineralogist, 82, 772-780.

Gwinner, M.P., 1971. Geolgie der Alpen. – Stuttgart, Schweizerbart'sche Verlags Buchhandlung, 477 p.

Handler, R., Genser, J., Friedl, G., Heidorn, R., Neubauer, F., Fritz, H. and Tenczer, V., 2000. ^{40}Ar-^{39}Ar ages of white mica from Austroalpine basement units along the TRANSALP section: Tectonic implications. 2nd international TRANSALP Colloquium, Munich, 17.

Harrison, T.M., Catlos, E. and Montel, J.M., 2002. U-Th-Pb dating of phosphate minerals. Reviews in Mineralogy and Geochemistry, 48, 523-577. http://dx.doi.org/10.2138/rmg.2002.48.14

Heinisch, H., 1981. Zum ordovizischen „Porphyroid"-Vulkanismus der Ost- und Südalpen – Stratigraphie, Petrographie, Geochemie. Jahrbuch der Geologischen Bundesanstalt, 124, 1-109.

Heinisch, H. and Schmidt, K., 1982. Zur Genese der Augengneise im Altkristallin der Ostalpen. Neues Jahrbuch für Geologie und Paläontologie Monatshefte, 1982, 211-239.

Janots, E., Engi, M., Berger, A., Allaz, J., Schwarz, J.O. and Spandler, C., 2008. Prograde metamorphic sequence of REE-minerals in pelitic rocks of the Central Alps: Implications on allanite-monazite-xenotime phase relations from 250 to 610°C. Journal of Metamorphic Geology, 26, 509-526. http://dx.doi.org/10.1111/j.1525-1314.2008.00774.x

Janots, E., Engi, M., Rubatto, D., Berger, A., Gregory, C. and Rahn, M., 2009. Metamorphic rates in collisional orogeny from in situ allanite and monazite dating. Geology, 37, 11-14. http://dx.doi.org/10.1130/G25192A.1

Jercinovic, M.J. and Williams, M.L., 2005. Analytical perils (and progress) in electron microprobe trace element analysis applied to geochronology: background acquisition, interferences, and beam irradiation effects. American Mineralogist, 90, 526-546.

King, P.L., White, A.J.R., Chappell, B.W. and Allan, C.M., 1997. Characterization and origin of aluminous A-type granites from the Lachlan Fold Belt, Southeastern Australia. Journal of Petrology, 38, 371-391.

Klötzli, U.S., Koller, F., Scharbert, S. and Höck, V., 2001. Cadomian lower-crustal contributions to Variscan granite petrogenesis (South Bohemian Pluton, Austria): constraints from zircon typology and geochronology, Whole-rock, and feldspar Pb-Sr isotope systematics. Journal of Petrology, 42, 1621-1642. http://dx.doi.org/10.1093/petrology/42.9.1621

Löschke, J., 1989. Lower Paleozoic volcanism of the Eastern Alps and its geodynamic implications. Geologische Rundschau, 78, 599-616.

Ludwig, K.R., 2003. Isoplot/Ex 3. A geochronological toolkit for Microsoft Excel. Berkeley Geochronology Center. Special Publication 4.

McDonough, W.F. and Sun, S.S., 1995. The composition of the Earth. Chemical Geology, 120, 223-253.

Mielke, P. and Winkler, H.G.F., 1979. Eine bessere Berechnung der Mesonorm für granitische Gesteine. Neues Jahrbuch für Mineralogie Monatshefte, 10, 471-480.

Miller C.F., McDowell S.M. and Mapes R.W., 2003. Hot and cold granites? Implications of zircon saturation temperatures and preservation of inheritance. Geology, 31, 529-532.

Neubauer, F., Frisch, W. and Hansen, B.T., 2002. Early Paleozoic tectonothermal events in basement complexes of the eastern Greywacke Zone (Eastern Alps): evidence from U-Pb zircon data. International Journal of Earth Sciences, 91, 775-786. http://dx.doi.org/10.1007/s00531-001-0254-7

Ondrejka, M., Uher, P., Putiš, M., Broska, I., Bačík, P., Konečný, P., and Schmiedt, I., 2012. Two-stage breakdown of monazite by post-magmatic and metamorphic fluids: An example from the Veporic orthogneiss, Western Carpathians, Slovakia. Lithos, 142, 245-255. http://dx.doi.org/10.1016/j.lithos.2012.03.012

Parrish, R.R., Roddick, J.C., Loveridge, W.D., Sullivan, R.W., 1987. Uranium-lead analytical techniques at the geochronology laboratory, Geological Survey of Canada. Geological Survey of Canada Paper, 87, 3-7.

Piber, A. 2002: Tectonometamorphic evolution of the Austro-Alpine nappes in the northern Zillertal-Area, Eastern Alps. Unpublished M.Sc. Thesis, University of Innsbruck, 268 p.

Piber A., 2005. The metamorphic evolution of the Austroalpine nappes north of the Tauern Window (Innsbruck Quartzphyllite Complex-Patscherkofel Crystalline Complex -Kellerjochgneiss and Wildschönau Schists). Unpublished Ph.D. Thesis, University of Innsbruck, 261 p.

Piber, A. and Tropper, P., 2003a. Preliminary eo-Alpine thermobarometric results of the Austroalpine crystalline basement nappes in the northwest of the Tauern Window between the Zillertal and the Wipptal (Eastern Alps, Tyrol). Arbeitstagung der Geologischen Bundesanstalt, 2003, 59-65.

Piber, A. and Tropper, P., 2003b. Multi-equilibrium thermobarometry in low grade metamorphic rocks from the Austroalpine nappes north of the Tauern Window (Kellerjochgneiss, Innsbruck Quartzphyllite). Memorie di Scienze Geologiche, 54, 227-231.

Piber, A. and Tropper, P., 2005. The polymetamorphic evolution of the Austroalpine Innsbruck Quartzphyllite Complex,

Mitteilungen der Österreichischen Mineralogischen Gesellschaft, 151, 103.

Piber, A. and Tropper, P., 2007. Muscovite-chlorite-quartz thermobarometry of the Permian metamorphic overprint of the central part of the western Innsbruck Quartzphyllite Complex (Tyrol, Austria). Mitteilungen der Österreichischen Mineralogischen Gesellschaft, 153, 291-300.

Piber, A. and Tropper, P., 2010. Tectonometamorphic evolution of the Austroalpine nappes in the northern Zillertal area (Tyrol, Eastern Alps). Geo.Alp, 7, 71-92.

Piber, A., Tropper, P. and Mirwald, P.W., 2009. Geothermobarometry of a stilpnomelane-garnet-bearing metapegmatite: P-T constraints on the eo-Alpine metamorphic overprint of the Austroalpine nappes north of the Tauern Window. Mineralogy and Petrology, 96, 99-111. http://dx.doi.org/10.1007/s00710-009-0046-5

Pichler, A., 1868. Beiträge zur Geognosie Tirols. Jahrbuch der K. u. K. Geologischen Reichsanstalt Wien.

Pupin, J.P., 1980. Zircon and granite petrology. Contributions to Mineralogy and Petrology, 73, 207-220.

Pyle, J.M. and Spear, F.S., 1999. Yttrium zoning in garnet: coupling of major and accessory phases during metamorphic reactions. Geological Materials Research 1, 1-49.

Pyle, J.M. and Spear, F.S., 2000. An empirical garnet (YAG)-xenotime thermometer. Contributions to Mineralogy and Petrology, 138, 51-58.

Pyle, J.M., Spear, F.S., Rudnick, R.L. and McDonough, W.F., 2001. Monazite-xenotime-garnet equilibrium in metapelites and a new monazite-garnet thermometer. Journal of Petrology 42, 2083-2107.

Rockenschaub, M., Kolenprat, B. and Frank, W., 1999. The tectonometamorphic evolution of Austroalpine units in the Brenner area (Tirol, Austria)-new geochronological implications. Tübinger Geowissenschaftliche Arbeiten Serie A, 52, 118-119.

Rockenschaub, M., Kolenprat, B. and Nowotny, A., 2003. Innsbrucker Quarzphyllitkomplex, Tarntaler Mesozoikum, Patscherkofelkristallin. Arbeitsberichte zur Arbeitstagung der Geologischen Bundesanstalt in Trins im Gschnitztal 2003, 41-58.

Roth, R., 1983. Petrographie und Tektonik der mittelostalpinen Kellerjochgneis-Decke und angrenzender Gebiete zwischen Schwaz und Märzengrund (Tirol.) Unpublished Ph.D. Thesis, University of Münster, 196 p.

Satir, M. and Morteani, G., 1978a. Kaledonische, herzynische und alpidische Ereignisse im Mittelostalpin nördlich der westlichen Hohen Tauern abgeleitet aus petrographischen und geochronologischen Untersuchungen, Geologische Rundschau, 68, 1-40.

Satir, M. and Morteani, G., 1978b. P-T conditions of the high-pressure Hercynian event in the Alps as deduced from petrological, Rb-Sr and O^{18}/O^{16} data on phengites from the Schwazer Augengneise (Eastern Alps, Austria), Schweizerische Mineralogische und Petrographische Mitteilungen, 58, 289-301.

Satir, M., Friedrichsen, H. and Morteani, G., 1980. $^{18}O/^{16}O$ and

D/H study of the minerals from the Steinkogelschiefer and the Schwazer Augengneis (Salzburg/Tirol, Austria), Schweizerische Mineralogische und Petrographische Mitteilungen, 60, 99-109.

Schauder, P., 2002. Ordovizische Entwicklung im Westabschnitt der Nördlichen Grauwackenzone unter besonderer Berücksichtigung mafischer und ultramafischer Magmatite. Geochemische, Isotopengeochemische und geochronologische Untersuchungen. Münchner Geologische Hefte, 30, 103 p.

Schindlmayr, A., 1999. Granitoids and Plutonic Evolution of the Ötztal-Stubai Massif – A Key for Understanding the Early Palaeozoic History of the Austroalpine Crystalline Basement in the Western Eastern Alps. Unpublished Ph.D. Thesis Salzburg University, 288 p.

Schmid, S. M., Fügenschuh, B., Kissling, E. and Schuster, R. 2004: Tectonic map and overall architecture of the Alpine orogen. Eclogae Geologae Helveticae, 97, 93-117.

Schmidegg, O., 1954. Achsen- und Flächengefüge beiderseits des Silltalbruches zwischen Innsbruck und Matrei, Tschermaks Mineralogisch Petrographische Mitteilungen, 4, 125-137.

Schmidegg, O., 1964. Die Ötztaler Schubmasse und ihre Umgebung. Verhandlungen der Geologischen Bundesanstalt, 1957/1, 76-77.

Schönlaub, H.P., 1980. Die Grauwackenzone In: Oberhauser, R. (ed.): Der geologische Aufbau Österreichs. Wien (Springer), 699 p.

Siebel, W., Raschka, H., Irber, W., Kreuzer, H., Lenz, K. L., Höhndorf, A. and Wendt, I., 1997. Early Palaeozoic acid magmatism in the Saxothuringian belt: new insights from a geochemical and isotopic study of orthogneisses and metavolcanic rocks from the Fichtelgebirge, SE: Germany. Journal of Petrology, 38, 203-30.

Söllner, F., Miller, H., and Höll, R., 1997. Alter und Genese der rhyodazitischen Metavulkanite ("Porphyroide") der Nördlichen Grauwackenzone und der Karnischen Alpen (Österreich): Ergebnisse von U/Pb Zirkondatierungen. Zeitschrift der Deutschen Geologischen Gesellschaft, 148/3-4, 499-522.

Sölva, H., Thöni, M. and Habler, G., 2003. Dating a single garnet crystal with very high Sm/Nd ratios (Campo basement unit, Eastern Alps). European Journal of Mineralogy, 15, 35-42. http://dx.doi.org/10.1127/0935-1221/2003/0015-0035

Spear, F.S., Pyle, J.M., 2002. Apatite, monazite and xenotime in metamorphic rocks. Reviews in Mineralogy and Geochemistry, 48, 293-335. http://dx.doi.org/10.2138/rmg.2002.48.7

Stacey, J.S. and Kramers, J.D., 1975. Approximation of terrestrial lead isotope evolution by a two-stage model. Earth and Planetary Science Letters, 26, 207-221

Steyrer, H.P. and Finger, F., 1996. Der Schwazer Augengneis: ein östlicher Ausläufer des Ötztal Kristallins? Mitteilungen der Österreichischen Mineralogischen Gesellschaft, 141, 226-227.

Thöni, M., Miller, C., Zanetti, A., Habler, G. and Goessler, W., 2008. Sm-Nd isotope systematics of high-REE accessory minerals and major phases: ID-TIMS, LA-ICP-MS and EPMA data constrain multiple Permian-Triassic pegmatite emplacement in the Koralpe, Eastern Alps. Chemical Geology, 254, 216-237.

http://dx.doi.org/10.1016/j.chemgeo.2008.03.008

Tollmann, A., 1963. Ostalpensynthese, Franz Deuticke, Vienna, 256 p.

Tollmann, A., 1977. Geologie von Österreich, Bd.1, Die Zentralalpen, Franz Deuticke, Vienna, 766 p.

Tollmann, A., 1986. Geologie von Österreich, Bd.3., Gesamtübersicht, Franz Deuticke, Vienna, 718 p.

Tropper, P. and Piber, A., 2012. Geothermobarometry of quartzphyllites, orthogneisses and greenschists of the Austroalpine basement nappes in the northern Zillertal (Innsbruck Quartzphyllite Complex, Kellerjochgneiss, Wildschönau Schists; Tyrol, Eastern Alps). Austrian Journal of Earth Sciences, 105, 80-94.

Von Raumer J.F., Bussy F., 2004. Mont Blanc and Aiguilles Rouges – Geology of their polymetamorphic basement. Memoires de Geologie (Lausanne), 42, 203 p.

Von Raumer, J. F., Bussy, F., Schaltegger, U., Schulz, B., and Stampfli, G. M., 2013. Pre-Mesozoic Alpine basements – their place in the European Paleozoic framework. Geological Society of America Bulletin, 125, 89-108. http://dx.doi.org/10.1130/B30654.1

Watson, E.B. and Harrison, T.M., 1983, Zircon saturation revisited: temperature and composition effects in a variety of crustal magma types: Earth and Planetary Science Letters, 64, 295-304.

Wendt, J.L. and Todt, W., 1991. A vapour digestion method for dating single zircons by direct measurement of U and Pb without chemical separation. Terra Abstracts, 3, 507-508

Wiedenbeck, M.P., Allè, P., Corfu, F., Griffin, W.L., Meier, M., Oberli, F., Von Quadt, A., Roddick, J.C., and Spiegel, W.,1995. Three natural zircon standards for U-Th-Pb Lu-Hf trace element and REE analysis. Geostandards Newsletter, 19, 1-23.

Peter TROPPER[1] [*], Friedrich FINGER[2], Erwin KRENN[2], Urs KLÖTZLI[3], Andreas PIBER[1] & Sonja GANGL[1]

[1] Institute of Mineralogy and Petrography, University of Innsbruck, Innrain 52, A-6020 Innsbruck, Austria;

[2] Department of Geography, Geology and Mineralogy, University of Salzburg, Helbrunnerstrasse 54, A-5020 Salzburg, Austria;

[3] Department of Lithospheric Research, University of Vienna, Althanstrasse 14, A-1090 Wien, Austria;

[*] Corresponding author: peter.tropper@uibk.ac.at